British Columbia radiogenic isotope compilation (Sr-Nd-Hf-Pb): Introduction and examples of utility

Alexei S. Rukhlov[1, a], Luke Ootes[1], and Tian Han[1]

[1] British Columbia Geological Survey, Ministry of Mining and Critical Minerals, Victoria, BC, V8W 9N3
[a] corresponding author: Alexei.Rukhlov@gov.bc.ca

Recommended citation: Rukhlov, A.S., Ootes, L., and Han, T., 2025. British Columbia radiogenic isotope compilation (Sr-Nd-Hf-Pb): Introduction and examples of utility. In: Geological Fieldwork 2024, British Columbia Ministry of Mining and Critical Minerals, British Columbia Geological Survey Paper 2025-01, pp. 177-188.

Abstract

Isotopic tracer ratios are powerful tools to map terrane boundaries, evaluate terrane evolution, and establish magmatic sources, and have become increasingly important in predictive mineral exploration. As part of province-wide geochemical re-analysis efforts, the British Columbia Geological Survey is generating hundreds of new whole rock radiogenic isotope data (Sr-Nd-Hf-Pb) from archived igneous rocks. The first iteration of a province-wide radiogenic isotope compilation includes previously published results from 1465 samples and will serve as a framework for ongoing analytical work. Isotope development and correlation diagrams ($\varepsilon_{Nd}(T)$, $\varepsilon_{Hf}(T)$, initial $^{87}Sr/^{86}Sr$, initial $^{206}Pb/^{204}Pb$, $^{207}Pb/^{204}Pb$, $^{208}Pb/^{204}Pb$) from the Cordillera provide insights into the evolution of the western margin of Laurentia and the accreted terranes to the west. These data highlight the location of terrane boundaries both today and through time, and provide diagnostic evidence of terrane evolution and magmatic sources.

Keywords: Sr-Nd-Hf-Pb isotopes, igneous rocks, terranes, mineral exploration

1. Introduction

Radiogenic isotope systematics (Rb-Sr, Sm-Nd, Lu-Hf, Th-Pb, and U-Pb) constrain absolute ages of rocks and minerals, fingerprint sources of mineralization and host rocks, and provide insights into evolution of terrestrial reservoirs (e.g., Amelin et al., 1999; Dhuime et al., 2015). In contrast to stable isotopes (^{86}Sr, ^{144}Nd, ^{177}Hf, and ^{204}Pb), the relative abundances of radiogenic or 'daughter' isotopes (^{87}Sr, ^{143}Nd, ^{176}Hf, ^{206}Pb, ^{207}Pb, and ^{208}Pb) change due to the decay of 'parent' isotopes (^{87}Rb, ^{147}Sm, ^{176}Lu, ^{238}U, ^{235}U, and ^{232}Th). As such, radiogenic isotope ratios represent time-integrated proxies of the parent-daughter (Rb/Sr, Sm/Nd, Lu/Hf, Th/Pb, and U/Pb). In contrast to elemental ratios that reflect partitioning of trace elements during magma evolution, closed system radiogenic isotopic ratios describe the source of a melt when it formed. Therefore, isotopic tracer ratios are powerful tools to map terranes and refine terrane history and have become increasingly important in predictive mineral exploration.

Since early application of initial $^{87}Sr/^{86}Sr$ ratios (e.g., Beddoe-Stephens and Lambert, 1981; Armstrong, 1988) and compilation of galena Pb isotopic data (Godwin et al., 1988), numerous studies have reported radiogenic isotopic data from the Canadian Cordillera (e.g., Ghosh and Lambert, 1989; Mihalynuk et al., 1992; Ghosh, 1995; Smith et al., 1995; Smith and Thorkelson, 2002; Sack et al., 2020) and neighbouring crustal reservoirs such as the Canadian Shield (Mitchell et al., 2010) and Siletz oceanic plateau (Phillips et al., 2017). Hundreds of new radiogenic isotopic data are currently being determined from historical samples as part of an ongoing province-wide project to re-analyze samples stored in the British Columbia Geological Survey rock archive using modern methods. As the first step in generating a comprehensive modern compilation for the entire province, Han et al. (2025) assembled previously published whole rock and mineral Sr-Nd-Hf-Pb and galena Pb isotopic data to serve as a framework for ongoing re-analysis work. This first iteration includes currently available data from 1465 samples (Fig. 1). Herein we describe how the compilation is being constructed and how it can be applied to address terrane boundaries and magma sources in the Canadian Cordillera.

2. Construction of the radiogenic isotope database

The BCGS data products are generated as tabular data files, where each row corresponds to a sample and each column holds attribute values (Fig. 2; Han et al., 2020). The data model is the basis of metadata capture with the use of in-house dictionary guides; the data model is used to produce a simplified data product (e.g., Han et al., 2020). Considering the similarities between the radiogenic isotope and geochronological data, instead of building a separate database, we extended the existing database for geochronology (Han et al., 2020) to house the compiled radiogenic isotope data. The extension was made by adding metadata attributes to the related identities without changing any between-identity relationships. We also added a new entity: code_geol, to record the names of the geologists who collected the samples. This addition allows the data model to be consistent with other data models designed for rock geochemistry and Regional Geochemical Survey. All the metadata are compatible with BC Digital Geology (Cui et al., 2017). Storing the geochronology and radiogenic

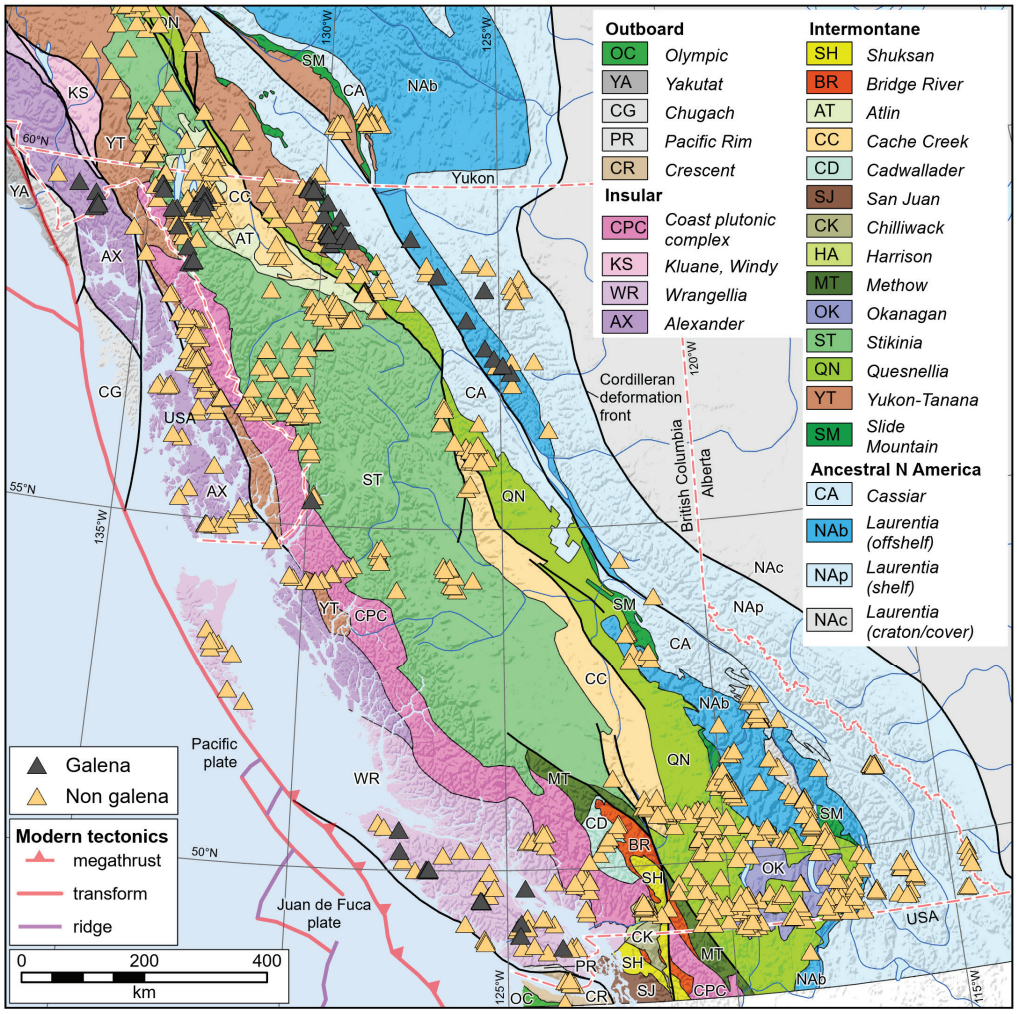

Fig. 1. Distribution of the radiogenic tracer isotope samples in Han et al. (2025). Terranes modified from Colpron (2020).

isotope data in the same database saves effort in future data management, eliminates duplications, and ensures data updates are synchronized. In the data model, measured isotopic ratios are captured from the source publication (e.g., Smith et al., 1995), whereas calculated values such as $^{87}Rb/^{86}Sr$, initial $^{87}Sr/^{86}Sr$, $\varepsilon_{Nd}(T)$, are generated on-the-fly if required in the output data products.

3. Methods

3.1. Isotopic ratios

Corrected for mass-fractionation to canonical values of stable or invariant isotopic ratios (e.g., $^{86}Sr/^{88}Sr$=0.1194, $^{146}Nd/^{144}Nd$=0.7219), radiogenic isotope ratios represent time-integrated proxies of the parent/daughter ratios such as Rb/Sr, Sm/Nd, Lu/Hf, Th/Pb, and U/Pb. In addition to geochronology and other metadata of related provincial data sets, the radiogenic isotopic compilation captures measured $^{87}Sr/^{86}Sr$, $^{143}Nd/^{144}Nd$, $^{176}Hf/^{177}Hf$, $^{206}Pb/^{204}Pb$, $^{207}Pb/^{204}Pb$, and $^{208}Pb/^{204}Pb$ ratios (Figs. 2-4), along with their instrumental or within-run uncertainties, type of sample (i.e., whole-rock or mineral fractions), ratio-specific analytical method, laboratory, and other details (Han et al., 2025). These metadata are captured from original publications.

Laboratory measured radiogenic isotope ratios (e.g., $^{143}Nd/^{144}Nd$) are typically back-corrected for time since formation, e.g., the crystallization age of an igneous intrusion, and this represents the initial ratio. Initial $^{87}Sr/^{86}Sr$ ratios were calculated using a decay constant of ^{87}Rb of $1.3968 \cdot 10^{-11}$ a^{-1} (Rotenberg et al., 2012). Initial $^{143}Nd/^{144}Nd$ ratios were recast as $\varepsilon_{Nd}(T)$ notation (Fig. 3), which is the relative difference in parts per 10^4 (epsilon, ε) between a sample and a reference such as the chondritic uniform reservoir (CHUR; Jacobsen and Wasserburg, 1980; Hamilton et al., 1983). Hence, positive $\varepsilon_{Nd}(T)$ values (e.g., in mantle-derived rocks) are referred to as 'super-chondritic' and negative ones such as in continental crust are 'sub-chondritic'. Initial $^{143}Nd/^{144}Nd$ ratios and $\varepsilon_{Nd}(T)$ values were calculated using a decay constant of ^{147}Sm of $6.539 \cdot 10^{-12}$ a^{-1} (Lugmair and Marti, 1978) and the CHUR (Jacobsen and Wasserburg, 1980; Hamilton et al., 1983). Initial $^{206}Pb/^{204}Pb$, $^{207}Pb/^{204}Pb$, and $^{208}Pb/^{204}Pb$ ratios were calculated using decay constants of ^{235}U of $9.8485 \cdot 10^{-10}$ a^{-1} and ^{238}U of $1.55125 \cdot 10^{-10}$ a^{-1} (Jaffey et al., 1971) and ^{232}Th of $4.9475 \cdot 10^{-11}$ a^{-1} (Le Roux and Glendenin, 1963).

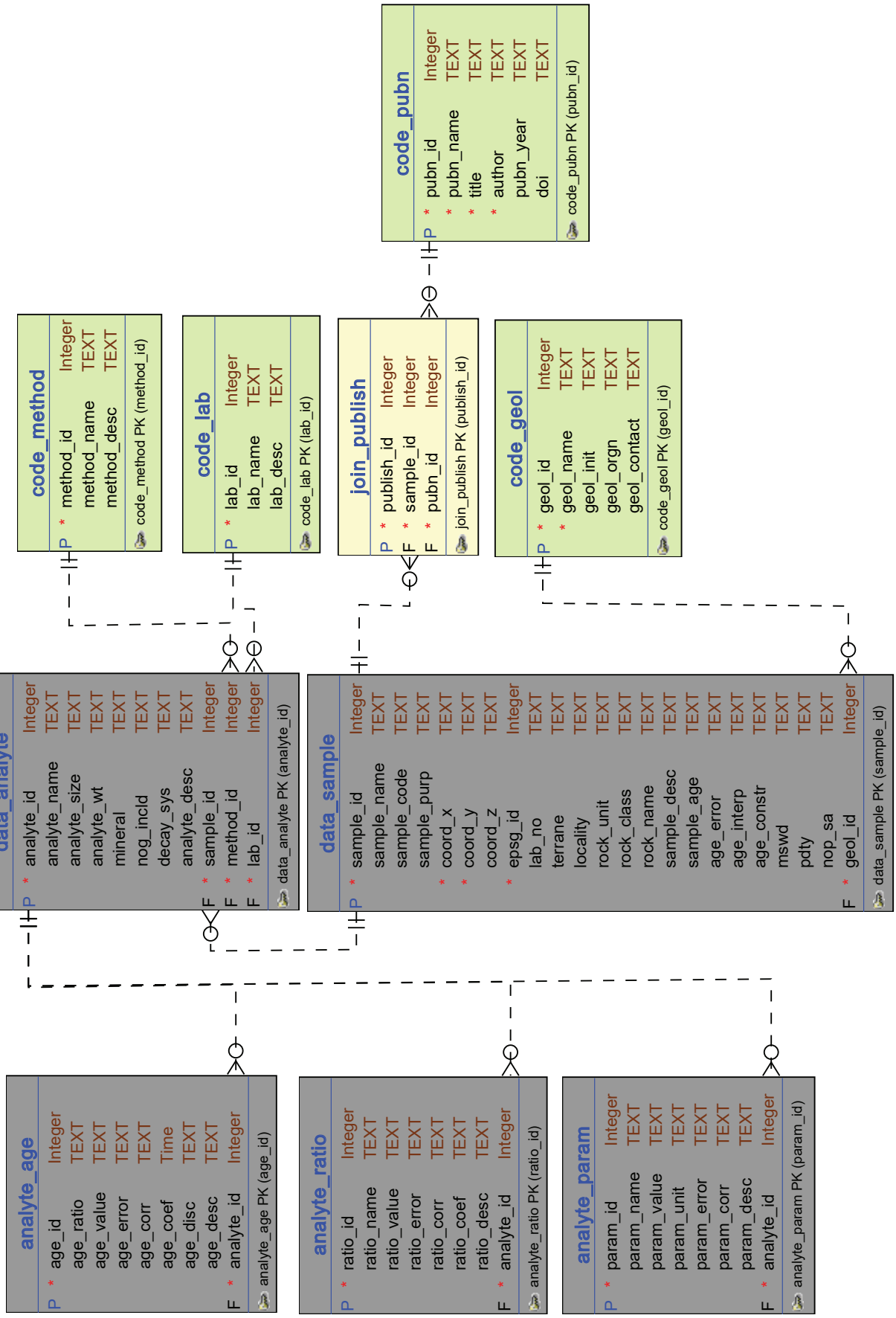

Fig. 2. Logical data model for the radiogenic isotope compilation. This data model is guided by an in-house data dictionary and used to produce simplified data products for release to the public (e.g., Han et al., 2020).

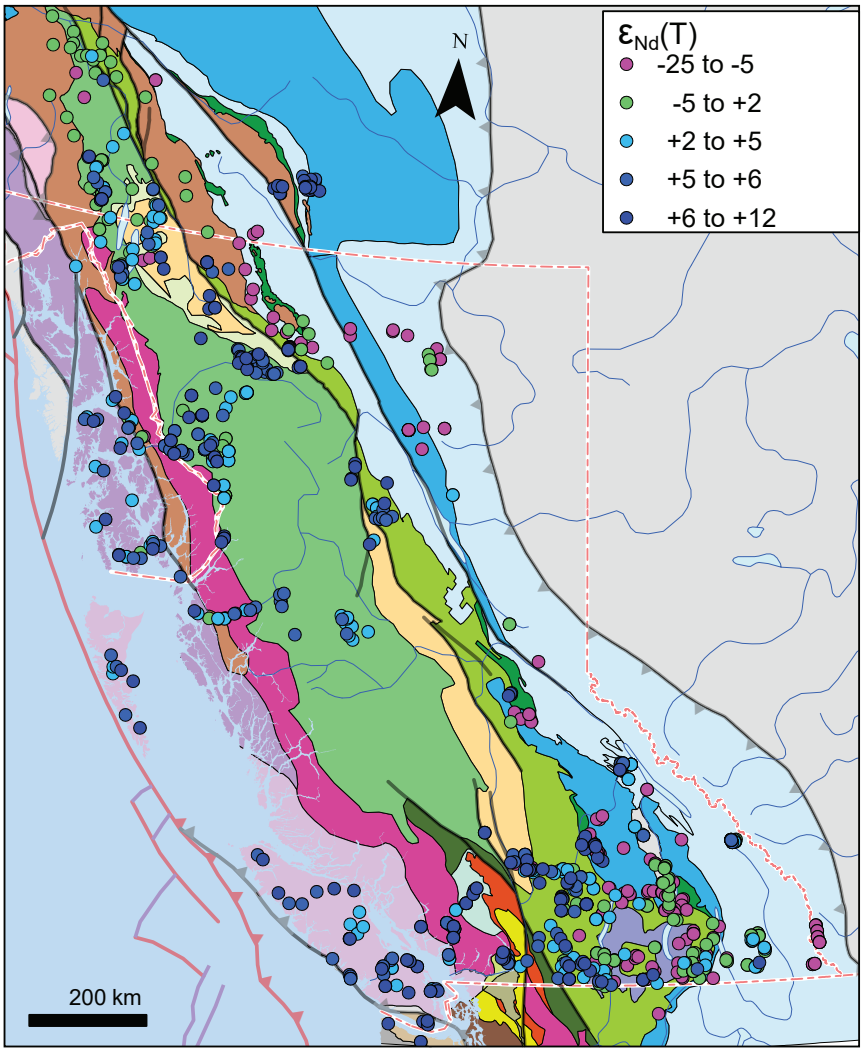

Fig. 3. Initial $^{143}Nd/^{144}Nd$ values in terms of $\varepsilon_{Nd}(T)$ notations in whole-rock and various mineral fractions (n=1047); $\varepsilon_{Nd}(T)=[(^{143}Nd/^{144}Nd_{sample}/^{143}Nd/^{144}Nd_{CHUR}) - 1]\cdot10^4$, where $^{143}Nd/^{144}Nd_{sample}$ is the initial ratio in the sample and $^{143}Nd/^{144}Nd_{CHUR}$ is the ratio in the chondritic uniform reservoir (CHUR; after Jacobsen and Wasserburg, 1980; Hamilton et al., 1983) at that time. Terranes as in Figure 1.

3.2. Terrane assignments

Terrane assignments (Figs. 5-8) were derived from geographic sample locations (Fig. 1). By this method, samples from post-accretionary rocks, generally accepted as <175 Ma, were also assigned to the older terrane (e.g., Quesnel) that underly the sample location. Locally, this is subjective and could change with new geological information that could require modification of terrane boundaries. As such, this information is not captured in the data compilation and users are encouraged to make their own decisions from knowledge of the Cordilleran orogen and the data itself.

4. Utility of radiogenic isotope compilation

Isotopic tracer ratios such as $^{87}Sr/^{86}Sr$, $^{143}Nd/^{144}Nd$, $^{176}Hf/^{177}Hf$, $^{206}Pb/^{204}Pb$, $^{207}Pb/^{204}Pb$, and $^{208}Pb/^{204}Pb$ are powerful tools to map terranes and refine terrane history (e.g., Godwin and Sinclair, 1982; Mitchell et al., 2010; Blanchet, 2019; Sack et al., 2020; Ootes et al., 2022; Curtis and Thiel, 2021; Dickin, 2023; Jones et al., 2023). These ratios have also become increasingly important in predictive mineral exploration (e.g., Gulson, 1986; Godwin et al., 1988; Bell and Franklin, 1993; Bell and Murton, 1995; Simonetti et al., 1996; Hussein et al., 2003; Rukhlov and Ferbey, 2015; Rukhlov et al., 2020; Sack et al., 2020; Osei et al., 2021; Lu et al., 2022). Below we highlight how the initial compilation (Han et al., 2025) can be used to identify terrane boundaries, consider terrane evolution, and examine the sources of post-Triassic magmatism in the Canadian Cordillera.

4.1. Identification of terrane boundaries

The $\varepsilon_{Nd}(T)$ decrease (Fig. 3) and initial $^{87}Sr/^{86}Sr$ ratios increase (Fig. 4) eastward, are attributed to the distance from the modern subduction zone, the nature of underlying terranes, and the thickness of lithosphere (Armstrong, 1988;

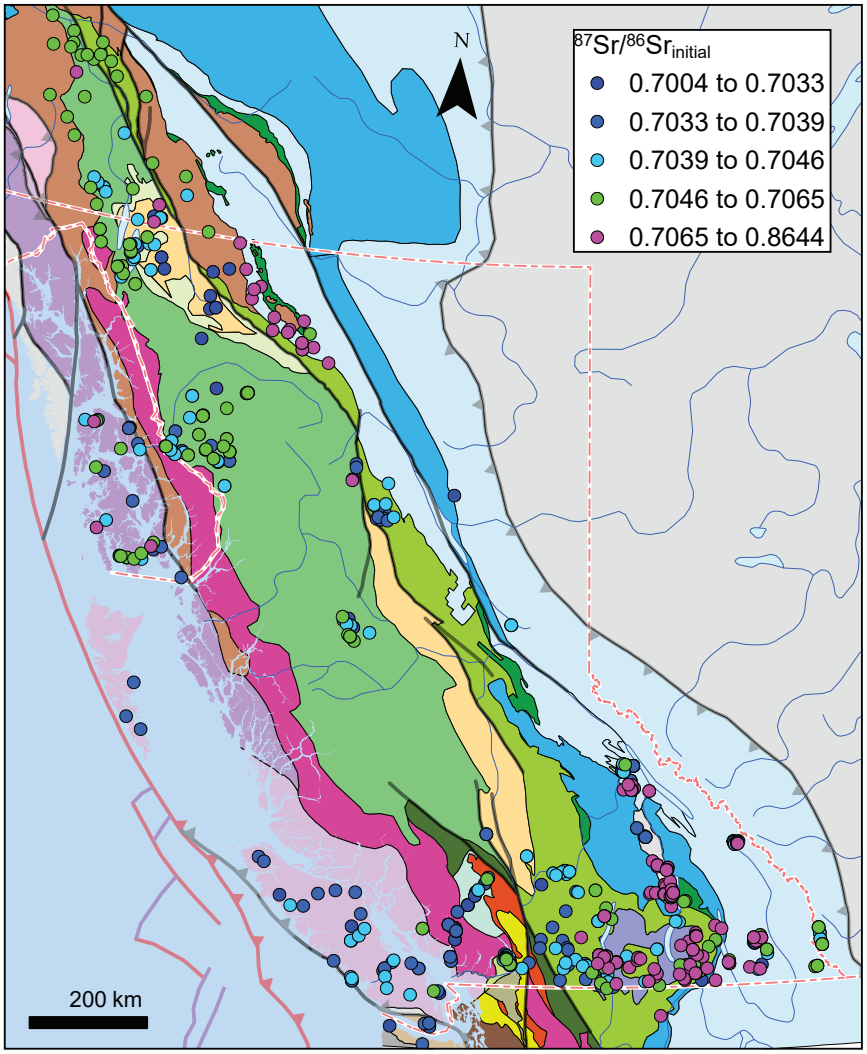

Fig. 4. Initial $^{87}Sr/^{86}Sr$ values in whole-rock and various mineral fractions (n=720). Terrane as in Figure 1.

Ghosh, 1995). The $\varepsilon_{Nd}(T)$ record from Mesoproterozoic to Triassic sedimentary rocks indicates at least two distinct sources of Archean and Proterozoic crustal residence age (Ghosh and Lambert, 1989). Igneous rocks record a change from juvenile character (i.e., super-chondritic $^{143}Nd/^{144}Nd$ and low $^{87}Sr/^{86}Sr$ ratios of <0.7045) during the Late Triassic-Early Jurassic to more craton-influenced by the Middle Jurassic (i.e., sub-chondritic $^{143}Nd/^{144}Nd$ and $^{87}Sr/^{86}Sr$ ratios >0.7041; Figs. 3-6). Ghosh (1995) interpreted that eastern Quesnel terrane marked the western boundary of the North American basement from the Middle Jurassic to Cenozoic (Figs. 3, 4). Similarly, Mihalynuk et al. (1992) ruled out North American basement for both the Cache Creek and Stikine terranes based on Sr isotopic evidence, a finding that was recently corroborated by Hf isotopic data in zircon for eastern Stikine (e.g., Ootes et al., 2022) and north-central Quesnel terranes (Jones et al., 2023).

4.2. Terrane evolution

Isotope development diagrams (time versus $\varepsilon_{Nd}(T)$ and initial $^{87}Sr/^{86}Sr$; Figs. 5, 6) for igneous rocks from the northern Cordillera provide insights into the evolution of the western margin of Ancestral North America and the accreted terranes to the west (Figs. 1, 3, 4). The isotopic data reveal generally juvenile sources for volcanic arcs that are older than 200 Ma, including the Intermontane and Insular terranes. The convergence of the data arrays defined by the Intermontane terranes with the depleted (upper) mantle model after Rehkämper and Hofmann (1997) is consistent with models that suggest a juvenile origin for these terranes as intra-oceanic volcanic arcs formed in late Paleozoic to early Mesozoic (e.g., Mihalynuk et al., 1992; Smith et al., 1995). Recently reported isotopic data on detrital and igneous zircons confirm that both the Intermontane and Insular terranes evolved from similar sources, formed on ocean floor during the late Paleozoic,

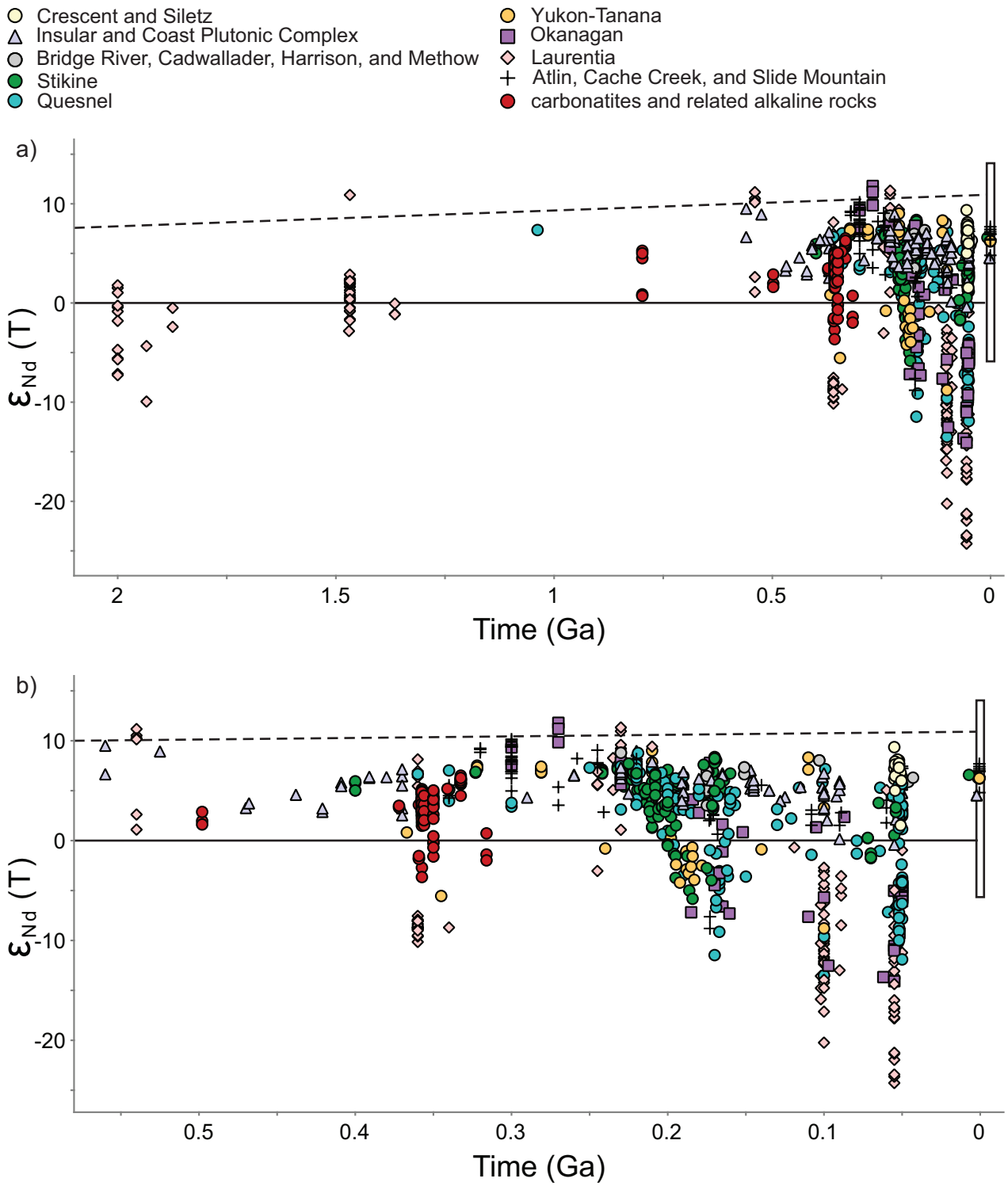

Fig. 5. Neodymium evolution diagram for whole-rock and mineral fractions of igneous rocks attributed to terranes, and carbonatites and related alkaline rocks. **a)** Time versus $\varepsilon_{Nd}(T)$; n=1056. **b)** Detail for Phanerozoic time versus $\varepsilon_{Nd}(T)$; n=990. $\varepsilon_{Nd}(T)=[(^{143}Nd/^{144}Nd_{sample}/^{143}Nd/^{144}Nd_{HUR}) - 1]\cdot 10^4$, where $^{143}Nd/^{144}Nd_{sample}$ is the initial ratio in the sample and $^{143}Nd/^{144}Nd_{CHUR}$ is the ratio in the chondritic uniform reservoir (CHUR, solid line; after Jacobsen and Wasserburg, 1980; Hamilton et al., 1983) at that time; depleted mantle model (dashed line) after Rehkämper and Hofmann (1997); the range of present-day $^{143}Nd/^{144}Nd$ values in mid-ocean ridge and ocean island basalts (rectangle) after Hart et al. (1992), Stracke et al. (2005), and Stracke (2012).

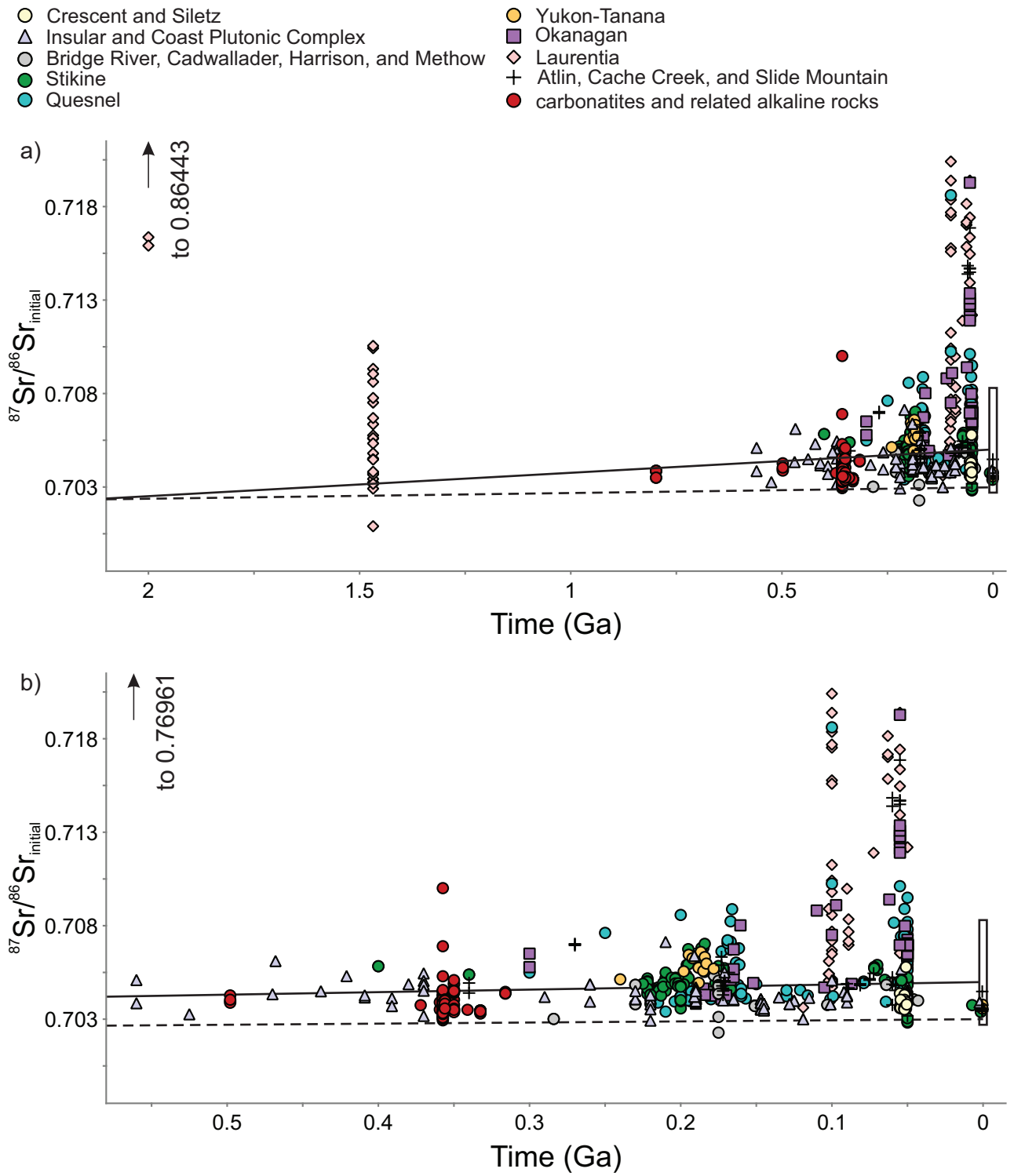

Fig. 6. Strontium evolution diagram for whole-rock and mineral fractions of igneous rocks attributed to terranes, and carbonatites and related alkaline rocks. **a)** Time versus initial $^{87}Sr/^{86}Sr$; n=728; extremely radiogenic initial $^{87}Sr/^{86}Sr$ values (up to 0.86443) in metamorphic rocks of the Monashee Complex (ca. 2 Ga) of western Laurentia (Parkinson, 1991). **b)** Detail for Phanerozoic time versus initial $^{87}Sr/^{86}Sr$; n=684; extremely radiogenic initial $^{87}Sr/^{86}Sr$ values (up to 0.76961) in metamorphic rocks of the Cassiar batholith (ca. 0.1 Ga) of western Laurentia (Driver et al., 2000). Evolution curve for bulk Earth (solid line; after DePaolo and Wasserburg, 1976) assuming primordial $^{87}Sr/^{86}Sr$=0.6990 of basaltic achondrite best initial (BABI); depleted mantle model (dashed line) after Rehkämper and Hofmann (1997); the range of present-day $^{87}Sr/^{86}Sr$ values in mid-ocean ridge and ocean island basalts (rectangle) after Hart et al. (1992), Stracke et al. (2005), and Stracke (2012).

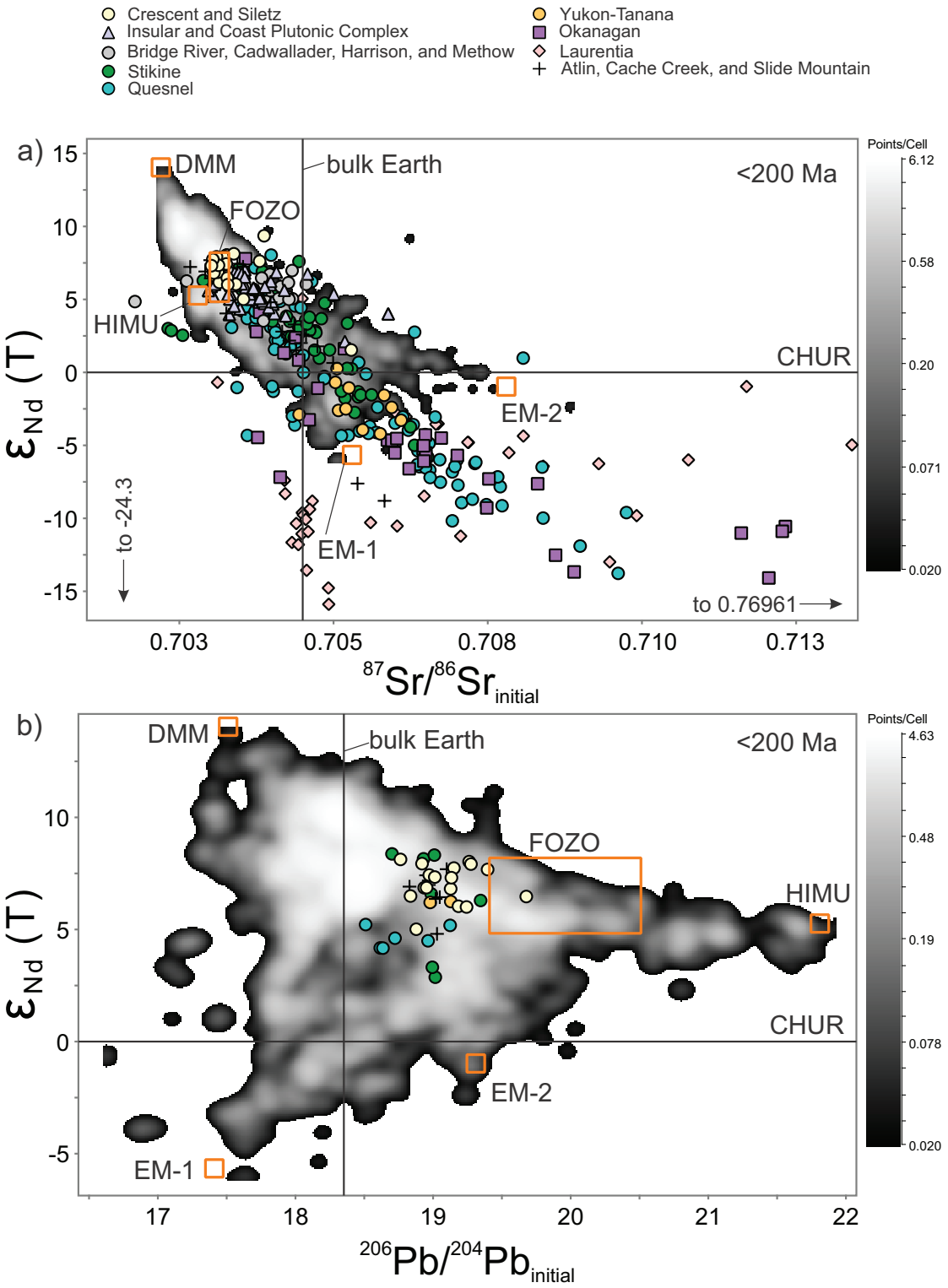

Fig. 7. Sr-Pb-Nd isotope correlation diagrams for <200 Ma igneous rocks by sample location in Cordilleran terranes; false-colour heat maps correspond to the density of data from global mid-ocean ridge and ocean island basalts (n=4939) after Stracke (2012). Depleted, mid-ocean ridge mantle (DMM), enriched mantle 1 and 2 (EM-1 and EM-2), 'FOcus ZOne' (FOZO), and high-$^{238}U/^{204}Pb$ or μ (HIMU) mantle components after Hart et al. (1992), Stracke et al. (2005), and Stracke (2012). **a)** Initial $^{87}Sr/^{86}Sr$ versus $\varepsilon_{Nd}(T)$; n=655; $\varepsilon_{Nd}(T)=[(^{143}Nd/^{144}Nd_{sample}/^{143}Nd/^{144}Nd_{CHUR}) - 1]\cdot 10^4$, where $^{143}Nd/^{144}Nd_{sample}$ is the initial ratio in the sample and $^{143}Nd/^{144}Nd_{CHUR}$ is the ratio in the chondritic uniform reservoir (CHUR; after Jacobsen and Wasserburg, 1980; Hamilton et al., 1983) at that time; present-day $^{87}Sr/^{86}Sr$ value for bulk Earth of 0.7045 after DePaolo (1988); extremely radiogenic initial $^{87}Sr/^{86}Sr$ values up to 0.76961 and low $\varepsilon_{Nd}(T)$ values (i.e., sub-chondritic initial $^{143}Nd/^{144}Nd$) to -24.3 in metamorphic rocks of the Cassiar batholith (ca. 0.1 Ga) of western Laurentia (Driver et al., 2000). **b)** Initial $^{206}Pb/^{204}Pb$ versus $\varepsilon_{Nd}(T)$; n=40; present-day $^{206}Pb/^{204}Pb$ value for bulk silicate Earth (BSE) of 18.34 after Allègre and Lewin (1989).

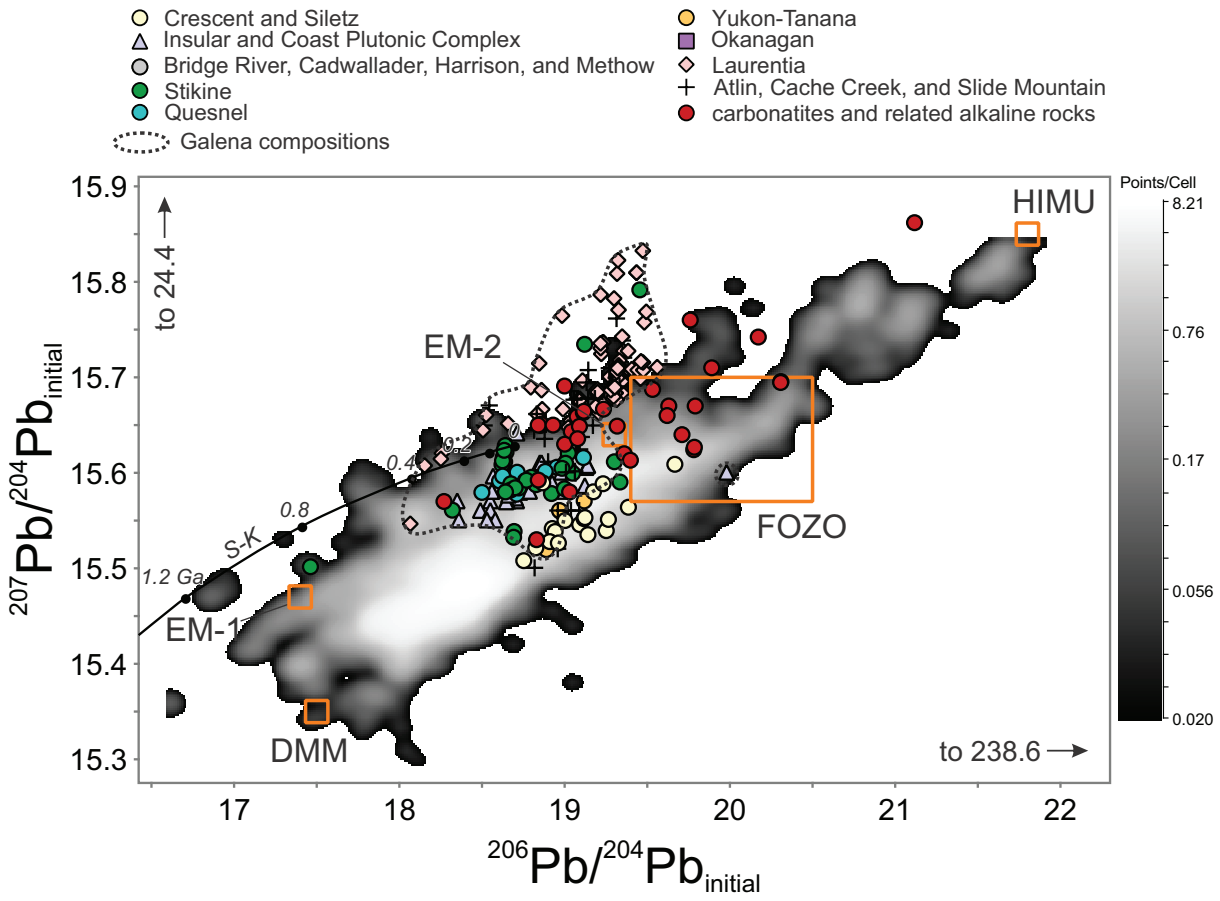

Fig. 8. Initial $^{206}Pb/^{204}Pb$ versus initial $^{207}Pb/^{204}Pb$ for whole-rock and mineral fractions (N=112) of carbonatites and related alkaline rocks, and other igneous rocks, and galena compositions (N=181, outlined by dotted line) attributed to terranes; false-colour heat maps correspond to the density of data from global mid-ocean ridge and ocean island basalts (n=4475) after Stracke (2012). Extremely radiogenic initial $^{206}Pb/^{204}Pb$ values up to 238.6 and initial $^{207}Pb/^{204}Pb$ up to 24.4 in apatite, carbonate, and molybdenite fractions from carbonatites of the Blue River area in east-central British Columbia after Rukhlov et al. (2018). Second-stage growth curve (S-K) for terrestrial lead isotopic evolution after Stacey and Kramers (1975). Depleted, mid-ocean ridge mantle (DMM), enriched mantle 1 and 2 (EM-1 and EM-2), 'FOcus ZOne' (FOZO), and high-$^{238}U/^{204}Pb$ or μ (HIMU) mantle components after Hart et al. (1992), Stracke et al. (2005), and Stracke (2012).

and evolved separately from Yukon-Tanana terrane and western Laurentia (Ootes et al., 2022; Jones et al., 2023). Much higher initial $^{87}Sr/^{86}Sr$ and extremely negative $\varepsilon_{Nd}(T)$ values of post-accretionary arcs reflect both terrane obduction over Ancestral North America (e.g., Smith et al., 1995) and perhaps contributions from subduction-modified upper mantle (Smith and Thorkelson, 2002). One of the important implications of the isotopic evidence is the lack of North American ancestry for some parts currently assigned to Ancestral North America (Figs. 3, 4). Such data can lead to new questions and potentially refine tectonic models. Below we discuss isotopic compositions of young (<200 Ma) igneous rocks from the northern Cordillera, because they can be directly compared with the oceanic signatures (Hart et al., 1992; Stracke et al., 2005; Stracke, 2012).

4.3. Identifying sources of post-Triassic magmatism in the Canadian Cordillera

Below we compare radiogenic isotopic data from <200 Ma igneous rocks with the mantle reference frame (Figs. 7, 8). We recognize that a fully rigorous assessment would exclude rocks that might have derived from continental crust, which evolved through multistep processes and are thus not directly comparable to mid-ocean ridge and ocean island basalts. Nonetheless, as a first approximation, we use all igneous rocks in the current compilation, limiting the time frame to <200 Ma, the age of the oldest preserved oceanic crust. The Sr-Nd-Pb isotopic data from <200 Ma igneous rocks partly overlap the mid-ocean ridge and ocean island basalts array (Fig. 7; Stracke, 2012). Post-accretionary igneous rocks (<175 Ma) emplaced into North American basement have values as low as $\varepsilon_{Nd}(T)$ -24.3 and extremely high $^{87}Sr/^{86}Sr$ (up to 0.76961; Fig. 7). Whole-rock and mineral fractions Pb, including Cordilleran carbonatites (Locock, 1994; Rukhlov et al., 2018; Çimen et al., 2019), partly overlap galena Pb compositions (Fig. 8). Again, juvenile compositions plot along the mantle array defined by the oceanic data (Fig. 8). Galena compositions from metallic mineral deposits along the western margin of Laurentia plot along or above the second-stage Pb growth curve of Stacey and Kramers (1975) (Fig. 8). These have

cratonic Pb isotopic signatures, characterized by the higher $^{207}Pb/^{204}Pb$ ratios at a given $^{206}Pb/^{204}Pb$ ratio than those of more juvenile compositions. Some data from carbonatites of the Blue River area, including molybdenite, have extremely radiogenic (high) initial Pb isotopic ratios (Rukhlov et al., 2018). Çimen et al. (2019) suggested a widespread, extremely radiogenic Pb mantle reservoir for the source of carbonatites from Blue River, Fen (Norway), and Shaxiongdong and Miaoya (China). However, Fen is the only anorogenic example in their comparison, and the data are not initial isotopic ratios (Andersen and Taylor, 1988). Global carbonatites from anorogenic settings lack such extremely high initial Pb isotopic compositions (e.g., Rukhlov et al., 2015). The examples from China and Blue River are metacarbonatites in orogenic belts (Chudy, 2013; Chen et al., 2018; Çimen et al., 2018) and Rukhlov et al. (2018) attributed the signatures in Blue River to Pb-loss from U-rich pyrochlore, and its concurrent sequestering into co-existing minerals such as apatite, carbonates, and molybdenite during metamorphism.

The depleted mid-ocean ridge mantle end-member (Fig. 8) represents shallow asthenospheric mantle, but it appears to have played a minimal role in the mantle source of the juvenile Cordilleran igneous rocks, including basalts of the Crescent-Siletz ocean plateau (Phillips et al., 2017). In contrast, the Sr-Pb-Nd data suggest a heterogeneous mantle source with mixing arrays involving the 'FOcus ZOne' (FOZO) mantle end-member (Figs. 7, 8) found in hot spots and considered to be relatively primitive and of deep mantle origin (Hart et al., 1992; Hauri et al., 1994; Bell and Tilton, 2002; Campbell and O'Neill, 2012).

Acknowledgment

We thank K. McLaren, T. Angelo, Q. Cunningham, F. de Waal, C. Torres, and D. Wegner for assisting with data compilation and quality control, and reviewers M.R. Cecil, R.A. Creaser, and K. Ansdell for many helpful comments.

References cited

Allègre, C.J., and Lewin, E., 1989. Chemical structure and history of the Earth, evidence from global non-linear inversion of isotopic data in a three-box model. Earth and Planetary Science Letters, 96, 61-88.

Amelin, Y., Lee, D.-C., Halliday, A.N., and Pidgeon, R.T., 1999. Nature of the Earth's earliest crust from hafnium isotopes in single detrital zircons. Nature, 399, 252-255.

Andersen, T., and Taylor, P.N., 1988. Pb isotope geochemistry of the Fen carbonatite complex, S.E. Norway: Age and petrogenetic implications. Geochimica et Cosmochimica Acta, 52, 209-215.

Armstrong, R.L., 1988. Mesozoic and early Cenozoic magmatic evolution of the Canadian Cordillera. In: Processes in Continental Lithospheric Deformation, Clark, S.P. Jr., Burchfiel, B.C., and Suppe, J., (Eds.), The Geological Society of America, Special Paper 218, pp. 55-92. <https://doi.org/10.1130/SPE218-p55>

Beddoe-Stephens, B., and Lambert, R.S.J., 1981. Geochemical, mineralogical, and isotopic data relating to the origin and tectonic setting of the Rossland volcanic rocks, southern British Columbia. Canadian Journal of Earth Sciences, 18, 858-868.

Bell, K., and Franklin, J.M., 1993. Application of lead isotopes to mineral exploration in glaciated terrains. Geology 21, 1143-1146.

Bell, K., and Murton, J.B., 1995. A new indicator of glacial dispersal: lead isotopes. Quaternary Science Reviews 14, 275-287.

Bell, K., and Tilton, G.R., 2002. Probing the mantle: the story from carbonatites. American Geophysical Union, Eos Transactions, 83, 273, 276-277.

Blanchet, C.L., 2019. A database of marine and terrestrial radiogenic Nd and Sr isotopes for tracing earth-surface processes. Earth System Science Data, 11, 741-759.

Campbell, I.H., and O'Neill, H.St.C., 2012. Evidence against a chondritic Earth. Nature, 483, 553-558.

Chen, W., Lu, J., Jiang, S.Y., Ying, Y.C., and Liu, Y.S., 2018. Radiogenic Pb reservoir contributes to the rare earth element (REE) enrichment in South Qinling carbonatites. Chemical Geology, 494, 80-95.

Chudy, T.C., 2013. The petrogenesis of the Ta-bearing Fir carbonatite system, east-central British Columbia, Canada. Unpublished Ph.D. thesis, University of British Columbia, Canada, 316 p.

Çimen, O., Kuebler, C., Monaco, B., Simonetti, S.S., Corcoran, L., Chen, W., and Simonetti, A., 2018. Boron, carbon, oxygen and radiogenic isotope investigation of carbonatite from the Miaoya complex, central China: Evidences for late-stage REE hydrothermal event and mantle source heterogeneity. Lithos, 322, 225-237.

Çimen, O., Kuebler, C., Simonetti, S.S., Corcoran, L., Mitchell, R.H., and Simonetti, A., 2019. Combined boron, radiogenic (Nd, Pb, Sr), stable (C, O) isotopic and geochemical investigations of carbonatites from the Blue River Region, British Columbia (Canada): Implications for mantle sources and recycling of crustal carbon. Chemical Geology, 529, article 119240. <https://doi.org/10.1016/j.chemgeo.2019.07.015>

Colpron, M., 2020. Yukon terranes-A digital atlas of terranes for the northern Cordillera. Yukon Geological Survey. <https://data.geology.gov.yk.ca/Compilation/2#InfoTab>

Cui, Y., Miller, D., Schiarizza, P., and Diakow, L.J., 2017. British Columbia digital geology. British Columbia Ministry of Energy, Mines and Petroleum Resources, British Columbia Geological Survey Open File 2017-8, 9 p.

Curtis, S., and Thiel, S., 2019. Identifying lithospheric boundaries using magnetotellurics and Nd isotope geochemistry: An example from the Gawler Craton, Australia. Precambrian Research, 320, 403-423. <https://doi.org/10.1016/j.precamres.2018.11.013>

DePaolo, D.J., 1988. Neodymium Isotopes in Geology. Springer-Verlag, 187 p.

DePaolo, D.J., and Wasserburg, G.J., 1976. Inferences about magma sources and mantle structure from variations of $^{143}Nd/^{144}Nd$. Geophysical Research Letters, 3, 743-746.

Dhuime, B., Wuestefeld, A., and Hawkesworth, C.J., 2015. Emergence of modern continental crust about 3 billion years ago. Nature Geoscience, 8, 552-555.

Dickin, A.P., 2023. The continuing power of Nd isotope mapping in Precambrian orogenic belts: A demonstration from the Ontario Grenville Province. Precambrian Research, article 107209. <https://doi.org/10.1016/j.precamres.2023.107209>

Driver, L.A., Creaser, R.A., Chacko, T., and Erdmer, P., 2000. Petrogenesis of the Cretaceous Cassiar batholith, Yukon-British Columbia, Canada: Implications for magmatism in the North American Cordilleran interior. Geological Society of America Bulletin, 112, 1119-1133.

Godwin, C.I., and Sinclair, A.J., 1982. Average lead isotope growth curves for shale-hosted zinc-lead deposits, Canadian Cordillera. Economic Geology, 77, 675-690.

Godwin, C.I., Gabites, J.E., and Andrew, A., 1988. Leadtable: a galena lead isotope database for the Canadian Cordillera, with

a guide to its use by explorationists. British Columbia Ministry of Energy, Mines and Petroleum Resources, British Columbia Geological Survey Paper 1988-4, 187 p.

Ghosh, D.K., 1995. Nd-Sr isotopic constraints on the interactions of the Intermontane Superterrane with the western edge of North America in the southern Canadian Cordillera. Canadian Journal of Earth Sciences, 32, 1740-1758.

Ghosh, D.K., and Lambert, R.S.J., 1989. Nd-Sr isotopic study of Proterozoic to Triassic sediments from southeastern British Columbia. Earth and Planetary Science Letters, 94, 29-44.

Gulson, B.L., 1986. Lead isotopes in mineral exploration. Developments in Economic Geology 23, Elsevier, Amsterdam, 245 p.

Hamilton, P.J., O'Nions, R.K., Bridgwater, D., and Nutman, A., 1983. Sm-Nd studies of Archaean metasediments and metavolcanics from West Greenland and their implications for the Earth's early history. Earth and Planetary Science Letters, 62, 263-272.

Han, T., Ootes, L., and Yun, K., 2020. The British Columbia Geological Survey geochronologic database: Preliminary release of ages. British Columbia Ministry of Energy, Mines and Low Carbon Innovation, British Columbia Geological Survey GeoFile 2020-10, 4 p.

Han, T., Ootes, L., Rukhlov, A.S., and Angelo, T., 2025. Radiogenic isotope compilation. British Columbia Ministry of Mining and Critical Minerals, British Columbia Geological Survey GeoFile 2025-08, in press.

Hart, S.R., Hauri, E.H., Oschmann, L.A., and Whitehead, J.A., 1992. Mantle plumes and entrainment: isotopic evidence. Science, 256, 517-520.

Hauri, E.H., Whitehead, J.A., and Hart, S.R., 1994. Fluid dynamic and geochemical aspects of entrainment in mantle plumes. Journal of Geophysical Research, 99(B12), 24275-24300.

Hussein, A.A., Lochner, C., and Bell, K., 2003. Application of Pb isotopes to mineral exploration in the Halfmile Lake area, Bathurst, New Brunswick. In: Massive Sulfide Deposits of the Bathurst Mining Camp, New Brunswick, and Northern Maine, Goodfellow, W.D., McCutcheon, S.R., and Peter, J.M., (Eds.), Economic Geology Monographs 11, pp. 679-688.

Jacobsen, S.B., and Wasserburg, G.J., 1980. Sm-Nd isotopic evolution of chondrites. Earth and Planetary Science Letters, 50, 139-155.

Jaffey, A.H., Flynn, K.F., Glendenin, L.E., Bentley, W.C., and Essling, A.M., 1971. Precision measurement of half-lives and specific activities of ^{235}U and ^{238}U. Physical Review, C4, 1889-1906.

Jones, G., Ootes, L., Luo, Y., Vezinet, A., Stern, R., Milidragovic, D., and Pearson, D.G., 2023. The relative roles of ancient and juvenile crust in building accretionary orogens-Minimal ancient crust involved in the magmatic evolution of a North American Cordillera accreted terrane indicated by igneous zircon Hf-O. Lithos, 452-453, article 107213. <https://doi.org/10.1016/j.lithos.2023.107213>

Le Roux, L.J., and Glendenin, L.E., 1963. Half-life of thorium-232. In: Proceedings of the National Conference on Nuclear Energy, Pretoria, South Africa, pp. 83-94.

Locock, A.J., 1994. Aspects of the geochemistry and mineralogy of the Ice River alkaline intrusive complex, Yoho National Park, British Columbia. Unpublished M.Sc. thesis, University of Alberta, Canada, 163 p.

Lu, Y.-J., Wingate, M.T.D., Champion, D., Smithies, R.H., Johnson, S.P., Gessner, K., Maas, R., Mole, D.R., Poujol, M., Zhao, J.-X., and Creaser, R.A., 2022. Samarium-neodymium isotope map of Western Australia. State of Western Australia, Department of Mines, Industry Regulation and Safety, Technical Report, 8 p. <https://insu.hal.science/insu-03817088v1>

Lugmair, G.W., and Marti, K., 1978. Lunar initial $^{143}Nd/^{144}Nd$: Differential evolution of lunar crust and mantle. Earth and Planetary Science Letters, 39, 349-357.

Mihalynuk, M.G., Smith, M.T., Gabites, J.E., Runkle, D. and Lefebure, D., 1992. Age of emplacement and basement character of the Cache Creek terrane as constrained by new isotopic and geochemical data. Canadian Journal of Earth Sciences, 29, 2463-2477.

Mitchell, R.K., van Breemen, O., Davis, W.J., and Buenviaje, R., 2010. Sm-Nd isotopic data from the Canadian Shield north of 60 degrees latitude, northern Canada. Geological Survey of Canada, Open File 6409, 15 p.

Ootes, L., Milidragovic, D., Friedman, R., Wall, C., Cordey, F., Luo, Y., Jones, G., Pearson, D.G., and Bergen, A., 2022. A juvenile Paleozoic ocean floor origin for eastern Stikinia, Canadian Cordillera. Geosphere, 18, 1297-1315. <https://doi.org/10.1130/GES02459.1>

Osei, K.P., Kirkland, C.L., and Mole, D.R., 2021. Nd and Hf isoscapes of the Yilgarn Craton, Western Australia and implications for its mineral systems. Gondwana Research, 92, 253-265. <https://doi.org/10.1016/j.gr.2020.12.027>

Parkinson, D., 1991. Age and isotopic character of Early Proterozoic basement gneisses in the southern Monashee Complex, southeastern British Columbia. Canadian Journal of Earth Sciences, 28, 1159-1168.

Phillips, B.A., Kerr, A.C., Mullen, E.K., and Weis, D., 2017. Oceanic mafic magmatism in the Siletz terrane, NW North America: Fragments of an Eocene oceanic plateau? Lithos, 274-275, 291-303.

Rehkämper, M., and Hofmann, A.W., 1997. Recycled ocean crust and sediment in Indian Ocean MORB. Earth and Planetary Science Letters, 147, 93-106.

Rotenberg, E., Davis, D.W., Amelin, Y., Ghosh, S., and Bergquist, B.A., 2012. Determination of the decay-constant of ^{87}Rb by laboratory accumulation of ^{87}Sr. Geochimica et Cosmochimica Acta, 85, 41-57.

Rukhlov, A.S., and Ferbey, T., 2015. Application of lead isotopes in till for mineral exploration: A simplified method using ICP-MS. British Columbia Ministry of Energy and Mines, British Columbia Geological Survey Paper 2015-2, 93 p.

Rukhlov, A.S., Bell, K., and Amelin, Y., 2015. Carbonatites, isotopes and evolution of the subcontinental mantle: An overview. In: Symposium on Strategic and Critical Materials Proceedings, November 13-14, 2015, Victoria, British Columbia, Simandl, G.J., and Neetz, M., (Eds.), British Columbia Ministry of Energy and Mines, British Columbia Geological Survey, Paper 2015-3, pp. 39-64.

Rukhlov, A.S., Chudy, T.C., Arnold, H., and Miller, D., 2018. Field trip guidebook to the Upper Fir carbonatite-hosted Ta-Nb deposit, Blue River area, east-central British Columbia. British Columbia Ministry of Energy, Mines and Petroleum Resources, Geological Survey GeoFile 2018-6, 67 p.

Rukhlov, A.S., Fortin, G., Kaplenkov, G.N., Lett, R.E., Lai, V.W.-M., and Weis, D., 2020. Multi-media geochemical and Pb isotopic evaluation of modern drainages on Vancouver Island. In: Geological Fieldwork 2019, British Columbia Ministry of Energy, Mines and Petroleum Resources, British Columbia Geological Survey Paper 2020-01, pp. 133-167.

Sack, P.J., Colpron, M., Crowley, J.L., Ryan, J.J., Allan, M.M., Beranek, L.P., and Joyce, N.L., 2020. Atlas of Late Triassic to Jurassic plutons in the Intermontane terranes of Yukon. Yukon Geological Survey, Open File 2020-1, 365 p.

Simonetti, A., Bell, K., and Hall, G.E.M., 1996. Pb isotopic ratios and elemental abundances for selective leachates from near-surface till: implications for mineral exploration. Applied Geochemistry, 11, 721-734.

Smith, A.D., and Thorkelson, D., 2002. Geochemical and Nd-Sr-Pb isotopic evidence on the origin and geodynamic evolution of mid-Cretaceous continental arc volcanic rocks of the Spences Bridge Group, south-central British Columbia. Geological Journal, 37, 167-186.

Smith, A.D., Brandon, A.D., and Lambert, R.S., 1995. Nd-Sr isotope systematics of Nicola Group volcanic rocks, Quesnel terrane. Canadian Journal of Earth Sciences, 32, 437-446.

Stacey, J.S., and Kramers, J.D., 1975. Approximation of terrestrial lead isotopic evolution by a two-stage model. Earth and Planetary Science Letters, 26, 207-221.

Stracke, A., 2012. Earth's heterogeneous mantle: a product of convection-driven interaction between crust and mantle. Chemical Geology, 330-331, 274-299.

Stracke, A., Hofmann, A.W., and Hart, S.R., 2005. FOZO, HIMU, and the rest of the mantle zoo. Geochemistry, Geophysics, Geosystems, 6, Q05007. <https://doi.org/10.1029/2004GC000824>